RSC Advances

PAPER

View Article Online
View Journal | View Issue

Cite this: *RSC Adv.*, 2024, **14**, 28915

Magnetic iron-based waterworks sludge modified by chitosan and FeS for aqueous Cr(VI) adsorption and reduction†

Jingxi Tie,‡[a] Weipeng Li,‡[a] Xiaohan Duan,‡[b] Huawen Wang,‡[a] Shuli Liu‡[a] and Weigao Zhao ‡*[c]

Heavy metals have been considered an evolving environmental concern due to their harmful and long-lasting impacts. We synthesized a composite of FeS/CS@MIBWS for aqueous Cr(VI) adsorption and reduction utilizing the iron-based waterworks sludge modified by chitosan and FeS. After determining the optimal conditions for the FeS/CS@MIBWS preparation, its Cr(VI) removal capability was evaluated using material characterisation and static Cr(VI) adsorption assays. Cr(VI) elimination by the composite was a pH-dependent process, with pH 2 being the optimum in the range of 2–10. The adsorption process was befitted a pseudo-second-order model, and the equilibrium results agreed well with the Langmuir model. The thermodynamics investigation showed that Cr(VI) removal by the composite has both spontaneous and endothermic nature. Considering the ionic effects, Cl^-, SO_4^{2-} and PO_4^{3-} decreased Cr(VI) elimination in the sequence of $Cl^- < SO_4^{2-} < PO_4^{3-}$. The key mechanisms for Cr(VI) elimination were physical and chemical adsorption, chelation, and Cr(VI) reduction into Cr(III). Furthermore, FeS/CS@MIBWS demonstrated steady reusability (removal effectiveness of 70% after 5 cycles). FeS/CS@MIBWS's rapid, high-performance, reusable, and easily separable adsorption properties make it a promising choice for heavy metal environmental cleaning.

Received 17th April 2024
Accepted 27th July 2024

DOI: 10.1039/d4ra02852j

rsc.li/rsc-advances

1 Introduction

The heavy metal pollution in wastewater has attracted widespread attention.[1] Chromium appearing in surface water, ground water and soil primarily originates from wide range of modern industries with the dominant forms of Cr(VI) and Cr(III) compounds,[2,3] and Cr(VI) has been reported to be carcinogenic, teratogenic, mutagenic and non-biodegradable.[4,5] Compared to Cr(III), Cr(VI) has a higher solubility and exists in the forms $Cr_2O_7^{2-}$, $HCrO_4^-$, and CrO_4^{2-}.[6,7] Chronic exposure to Cr(VI) can induce major human disorders and pose a considerable hazard to aquatic creatures even at a very low concentration.[8,9] As a result, considering the mutagenic, poisonous, and long-lasting impacts of aqueous Cr(VI), fixing the problem is critical.

Electrochemical approaches, photocatalytic treatment, membrane filtration, ion exchange, adsorption, and other techniques have been developed to control the harm caused by Cr(VI).[10–13] In a variety of technologies, adsorption has attracted the most attention due to its benefits such as ease of use, low cost, excellent performance, wide pH range, and so on.[14]

Iron-based waterworks sludge (IBWS) is a byproduct generated from drinking water treatment plants using iron-based coagulants for water processing. Fe in IBWS mainly exists in amorphous phases, endowing it with porosity and high adsorption capability for a variety of contaminants such as phosphorus and heavy metals, *etc.*.[15–18] Additionally, IBWS can be magnetized by calcination or hydrothermal treatment,[19,20] resulting in a rapid separation from solution upon adsorption. However, due to the low affinity between Fe and Cr(VI), the adsorption capacity of the IBWS for Cr(VI) removal is poor and may be improved by modification.

Chitosan (CS), a natural polysaccharide, has the world's second biggest yearly production,[21] and has been proved to be an effective adsorbent for numerous pollutants[22–24] due to its merits including degradability, high reactivity and charge density, biocompatibility, renewability, and harmless.[25–27] Given that the form of Cr(VI) in water was oxyanions, existing hydroxyl and amine groups in CS can easily react with Cr(VI) and achieve better adsorption ability.[28]

Furthermore, because Cr(III) is substantially less toxic than Cr(VI), lowering is a viable and safe technique of eliminating Cr(VI). FeS may be a suitable material for immobilizing Cr(VI), as

[a]*School of Environmental and Municipal Engineering, North China University of Water Resources and Electric Power, Zhengzhou, 450046, PR China*

[b]*Henan Vocational College of Water Conservancy and Environment, Zhengzhou 450008, PR China*

[c]*School of Environmental Science and Engineering, Tianjin University, Tianjin 300350, China. E-mail: zhaoweigao@tju.edu.cn*

† Electronic supplementary information (ESI) available. See DOI: https://doi.org/10.1039/d4ra02852j

‡ These authors contributed equally.

both Fe^{2+} and S^{2-} can act as reducing agents. Yang *et al.*, for example, developed nano-FeS and CMC-FeS for Cr(VI) removal, and the two materials efficiently converted $Cr_2O_7^{2-}$ into $Cr_{0.75}(OH)_3$.[29] As a result, injecting FeS is thought to achieve simultaneous magnetic and efficient purification of the composite in this investigation.

In this work, we synthesized a novel composite with the aim of immobilizing aqueous Cr(VI). We investigated the physico-chemical parameters by characterisation, assessed the composite's reduction ability towards Cr(VI), and proved the process of adsorption. The findings give detailed insight into the manufacture of adsorption materials as well as a reference for lowering Cr(VI) in water.

2 Materials and methods

2.1 Adsorbent preparation

MIBWS utilized in this research was prepared according to the procedures disclosed in our earlier study.[3] The adsorbents used in this study were prepared *via* a modification of the way described in the literature.[30] Briefly, 1 g CS and various amounts of MIBWS (0.5, 0.75, 1 and 1.25 g) were added into 100 mL $C_2H_4O_2$ solution (2.5%, v/v) then stirred and sonicated for 2 h for complete dissolution of CS and uniform dispersion of MIBWS. Then, 50 mL $FeSO_4 \cdot 7H_2O$ (20 g L^{-1}) was added into the mixture dropwise. Next, the mixture was agitated for 12 h before 50 mL Na_2S was added dropwise under a N_2 environment at 60 °C and mixed for 2 h. Following that, 5 mL glutaraldehyde was added to the mixture once it had cooled. After fully aging for 24 hours, the combination was reacted at 60 °C for another 3 h, and its pH was adjusted in succession with NaOH solution. Finally, the mixture was rinsed and dried at 70 °C in a vacuum for 12 h before sieving through 0.15 mm screen mesh to get four FeS/CS@MIBWS adsorbents prepared with varying MIBWS dosage.

The best MIBWS dosage determined in the Cr(VI) adsorption studies with the four adsorbents stated above was used to prepare several types of FeS/CS@MIBWSs with varying S^{2-} and Fe^{2+} dosages. The S^{2-} : Fe^{2+} mole ratio was kept at 2 : 1 for all the composites, and the other preparing techniques were the same as mentioned earlier.

2.2 Adsorbent characterization

The functional groups of FeS/CS@MIBWS before and after Cr(VI) adsorption were analyzed using Fourier transform infrared spectroscopy (FTIR, Nicolet IS50, Thermo fisher, USA) in the spectra range of 4000–400 cm^{-1}. The Brunauer–Emmett–Teller specific surface area (S_{BET}) and pore diameter distribution was measured using an automatic specific surface area analyzer (BELSORP-max, MicrotracBEL, Japan). The surface element and chemical state of MIBWS, FeS/CS@MIBWS before and after Cr(VI) adsorption were determined by X-ray photoelectron spectroscopy (XPS, Escalab 250Xi+, Thermo Fisher Scientific USA). The crystalline phases of MIBWS and FeS/CS@MIBWS were studied using an X-ray diffractometer (XRD, SmartLab SE, Rigaku, Japan) in the 2θ range of 5–90° with a step size of 0.02°. Magnetic properties of FeS/CS@MIBWS were studied using a vibrating sample magnetometer (VSM, Lake shore 7404, USA). The zero point charge (pH_{PZC}) was determined using a zeta potential meter (Particle Metrix GmbH, Germany). The surface morphology of the composite was recorded using a scanning electron microscope (SEM, Zeiss Genimi500, Germany), and the element content of it was analyzed using a X-ray fluorescence spectrometer (XRF, primus, Japan).

2.3 Cr(VI)-containing wastewater preparation

The Cr(VI)-containing wastewater used in the study was prepared by dissolving $K_2Cr_2O_7$ into the deionized water. 0.1 M HCl and NaOH solutions were used to adjust the pH of the artificial solution. All the chemical reagents utilized in this study were analytically pure.

2.4 Batch adsorption experiment

0.02 g adsorbent and 50 mL artificial wastewater was placed in a flask in a shaker at 120 rpm, which reacted at fixed time span and temperature. The remnant Cr(VI) in the supernate was detected by a UV-vis spectrophotometer (UV-5100, Yuanxi, China) using the method described in our previous study.[3] All the tests were conducted in triplicate, and the average value was used for analysis.

3 Results and discussion

3.1 Adsorbent preparation

Fig. 1a shows the Cr(VI) removal by four FeS/CS@MIBWS prepared with varying MIBWS doses, denoted as FeS/CS@MIBWS1, FeS/CS@MIBWS2, FeS/CS@MIBWS3, and FeS/CS@MIBWS4. The four composites showed Cr(VI) removal capacities of 77.13, 61.92, 50.47 and 41.47 mg g^{-1}, respectively, as the MIBWS increased from 0.5 to 1.25 g, while the corresponding saturation magnetic inductions were 0.46, 7.22, 7.71 and 14.80 emu g^{-1} (Fig. 1b). FeS/CS@MIBWS1 has the best Cr(VI) removal but the worst magnetism, resulting in poor separability following Cr(VI) removal in a magnetic field. Unlike FeS/CS@MIBWS1, spent FeS/CS@MIBWS2 separated from the aqueous solution in 10 s using a magnetic force, while removing less Cr(VI). As a result, 0.75 g MIBWS was established to be the optimal dosage for FeS/CS@MIBWS preparation, taking into account both Cr(VI) removal and magnetic separation of the spent composite.

As shown in Fig. 2a, Cr(VI) adsorption increased from 47.82 to 66.12 mg g^{-1} when the $FeSO_4$ dose for the composite preparation increased from 0 to 2 g, demonstrating that $FeSO_4$ may improve Cr(VI) adsorption. Because there was no discernible improvement in Cr(VI) adsorption with increasing $FeSO_4$ dose from 1.5 to 2 g, hence, 1.5 g $FeSO_4$ was determined to be the optimal dosage for FeS/CS@MIBWS preparation. As a result, the best mass ratio for FeS/CS@MIBWS preparation was MIBWS : CS : $FeSO_4 \cdot 7H_2O$ = 0.75 : 1 : 1.5 g. Compared to IBWS, which had a lower Cr(VI) adsorption of 1.23 mg g^{-1}, FeS/CS@MIBWS had a substantially greater Cr(VI) adsorption of 65.72 mg g^{-1},

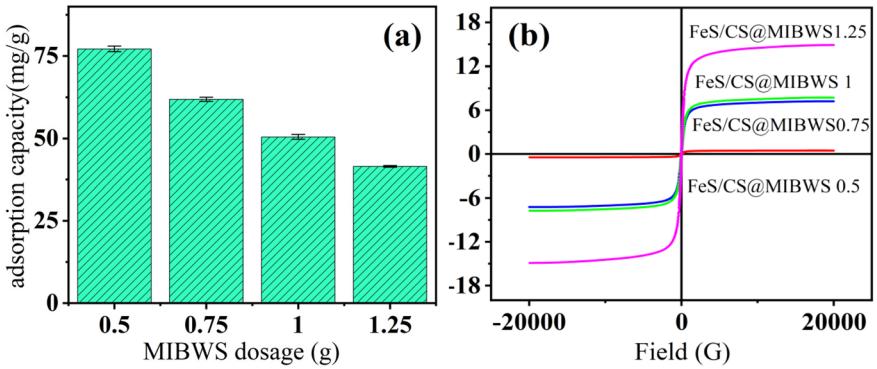

Fig. 1 Adsorption capacity of FeS/CS@MIBWS (a) and VSM (b) variation as function of MIBWS dosage (reaction time = 4 h, C_0 = 200 mg L^{-1}, T = 25 °C).

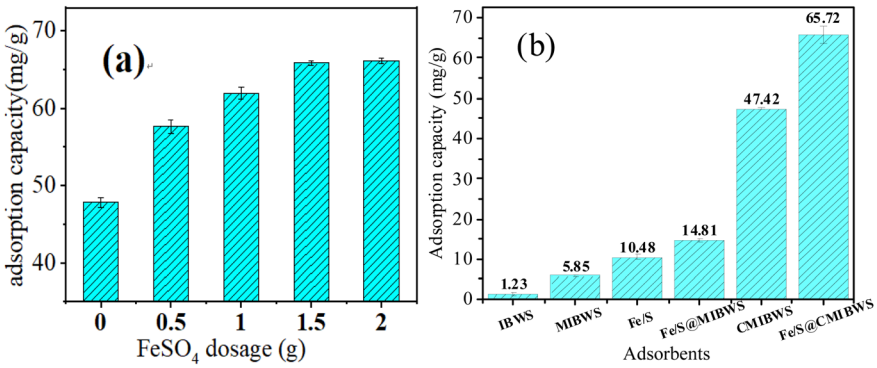

Fig. 2 Adsorption capacity of FeS/CS@MIBWS as a function of $FeSO_4 \cdot 7H_2O$ dosage in their ingredients (a); comparison of Cr(VI) adsorption by 6 adsorbents (b) (m = 0.02 g, T = 298 K, reaction time = 4 h, C_0 = 50 mg L^{-1}).

showing that the approach adopted in this work was effective for IBWS modification (Fig. 2a).

3.2 Characterization

The phase purity and crystallinity of the MIBWS and FeS/CS@MIBWS samples were analyzed by XRD (Fig. 3). The XRD patterns of MIBWS and FeS/CS@MIBWS were similar to each other, the characteristic XRD peaks at 2θ values of 30.2°, 35.6°, 43.3°, 57.3° and 62.8° were attributed to the (220), (311), (400), (511) and (440) crystal plane of Fe_3O_4 (JCPDS No. 19-0629).[31] Meanwhile, the diffraction pattern was in good agreement with the hexagonal phase of FeS (JCPDS Card No. 75-0602), and the peaks at 30.1°, 33.9°, 43.6°, 53.4° can be indexed to the (100), (101), (102), (110) planes of FeS, respectively.[32–36] The broad peak located at 20.40° were indexed to the semi-crystalline polymer of chitosan.[37,38]

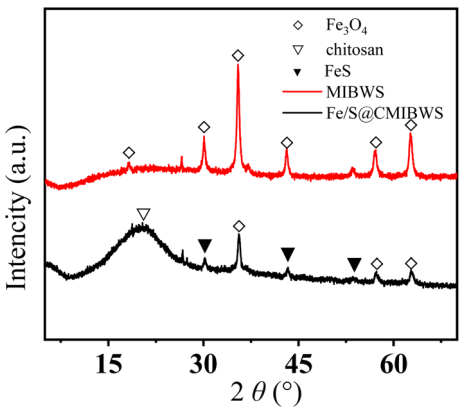

Fig. 3 XRD patterns of MIBWS and FeS/CS@MIBWS.

In our previous study,[3] pristine IBWS exhibited type IV N_2 adsorption–desorption isotherms with the usual type H3 hysteresis loop, whereas FeS/CS@MIBWS had the same kind of N_2 adsorption–desorption isotherms and hysteresis loop after modification (Fig. 4a).

As demonstrated in our previous study,[3] IBWS had S_{BET} of 115.34 m^2 g^{-1}, total pore volume (TPV) of 0.28 cm^3 g^{-1}, and average pore diameter (APD) of 9.75 nm, whereas, the corresponding parameters of FeS/CS@MIBWS were 27.05 m^2 g^{-1}, 0.32 cm^3 g^{-1}, and 14.54 nm, respectively (Fig. 4b and Table 1), indicating that modification by CS and FeS significantly reduced the surface area while increased the TPV and APD. IBWS had a greater S_{BET} than FeS/CS@MIBWS, but a lower Cr(VI) adsorption, demonstrating that S_{BET} was not the essential component in the adsorption process.

FeS/CS@MIBWS had a rough surface due to a high concentration of small particles (a), however there were a considerable

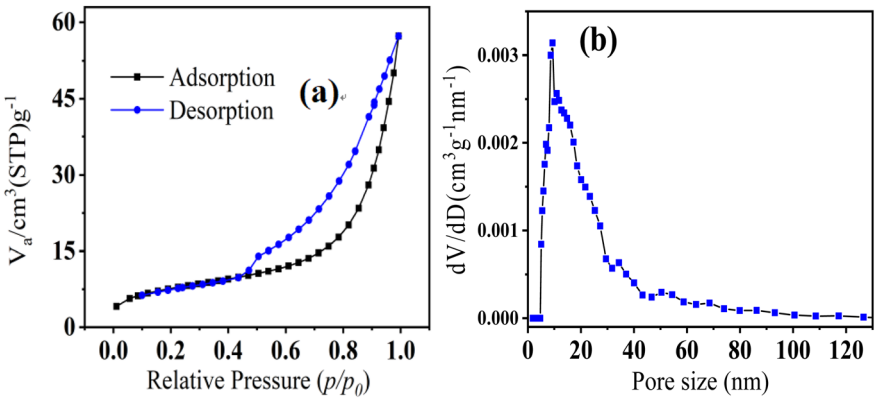

Fig. 4 Nitrogen physisorption–desorption isotherm (a) and pore size distribution (b) of FeS/CS@MIBWS.

Table 1 S_{BET} and pore parameters of FeS/CS@MIBWS

Sample	S_{BET} (m^2 g^{-1})	TPV (cm^3 g^{-1})	APD (nm)
Fe/S@CMIBWS	27.05	0.32	14.54

number of pores of varied sizes on its surface (b), as seen in Fig. 5. As demonstrated in Table 2, Fe, C, and S were the top three elements in FeS/CS@MIBWS, mostly derived from the IBWS before and after calcination, with FeS employed for modification.

3.3 Effect of working solution pH

Cr(VI) adsorption by FeS/CS@MIBWS reduced from 163.0 to 15.2 mg g^{-1} with the increasing pH from 2 to 10 (Fig. 6a), suggesting acidic environment was favorable for Cr(VI) elimination, which matched the previous studies.[39,40]

Fig. 6b shows that the pHpzc of FeS/CS@MIBWS was around pH 5.16. Protonation at pH < 5.16 positively charged the surface of FeS/CS@MIBWS, facilitating the electrostatic adsorption of the negatively charged oxyanions of Cr(VI) such as $HCrO_4^-$, $Cr_2O_7^{2-}$, and CrO_4^{2-}, whereas, negatively charged surface at pH > 5.16 repulsed the oxyanions in the solution, resulting in decreased Cr(VI) removal. Furthermore, the conflict between the oxyanions and hydroxyl groups for active points on the surface of FeS/CS@MIBWS reweakened Cr(VI) adsorption.[41,42]

3.4 Kinetic study

Fig. 7a shows that both of the two Cr(VI) adsorption processes increased as contact duration and Cr(VI) concentration raised. Furthermore, the two processes had initial rapid phases that were virtually at equilibrium at 360 minutes, and no additional substantial Cr(VI) removal was seen during the ensuing slow period. Pseudo-firstorder, pseudo-secondorder and Elovich models (eqn (1)–(3))[43,44] was utilized to further analyze the experimental data. Fig. 7b–d shows the linear fitting using the three models.

$$\log(q_e - q_t) = \log q_e - \frac{k_1}{2.303} t \quad (1)$$

$$\frac{t}{q_t} = \frac{t}{q_e} + \frac{1}{k_2 q_e^2} \quad (2)$$

Table 2 The main element content of FeS/CS@MIBWS

Element	Content (%)	Element	Content (%)
Fe	24.30	Mo	0.31
C	11.00	Na	0.24
S	7.02	K	0.16
Si	1.73	Mg	0.15
Al	0.81	Ti	0.10
Ca	0.36	Mn	0.05

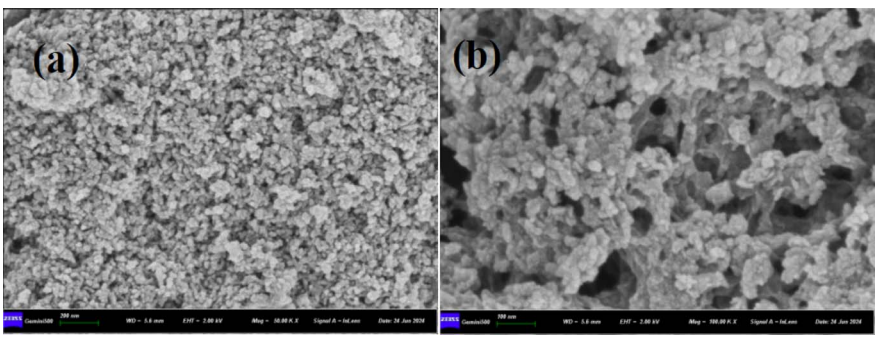

Fig. 5 SEM morphologies of FeS/CS@MIBWS magnified by 50 000 (a) and 100 000 times (b).

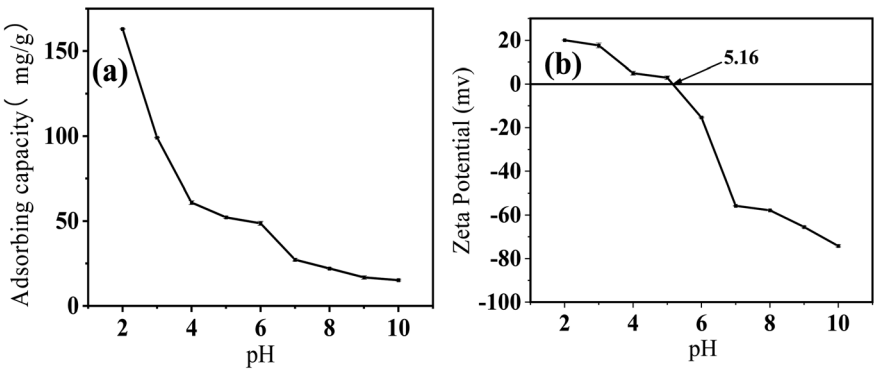

Fig. 6 Influence of the initial solution pH on Cr(VI) adsorption by FeS/CS@MIBWS (a), zeta potential analysis of FeS/CS@MIBWS (b).

$$q_t = \frac{1}{\beta}\ln(\alpha\beta) + \frac{1}{\beta}\ln t \quad (3)$$

where q_e (mg g^{-1}) and q_t (mg g^{-1}) were the Cr(VI) uptake at equilibrium and time t, respectively. k_1 (min^{-1}) and k_2 (g mg^{-1} min^{-1}) are the pseudo-first order and pseudo-second order rate constants, respectively. α (mg g^{-1} min^{-1}) and β (g mg^{-1}) are the initial adsorption rate and the desorption constant, respectively.

As shown in Table 3, the correlation coefficient (R^2) of the pseudo-second order model was higher than those of the other two models, and was closest to 1, suggesting that it was the optimal model to depict Cr(VI) adsorption on FeS/CS@MIBWS, and chemisorption was the rate-limiting step for the adsorption process in which electrons sharing or exchange between Cr(VI) and FeS/CS@MIBWS was involved.

3.5 Isotherms and thermodynamics study

Langmuir and Freundlich models (eqn (4) and (5))[45] were used to further understand the interaction between Cr(VI) and FeS/CS@MIBWS.

$$\frac{c_e}{q_e} = \frac{1}{q_m b} + \frac{c_e}{q_m} \quad (4)$$

$$\log q_e = \log k_f + \frac{1}{n}\log c_e \quad (5)$$

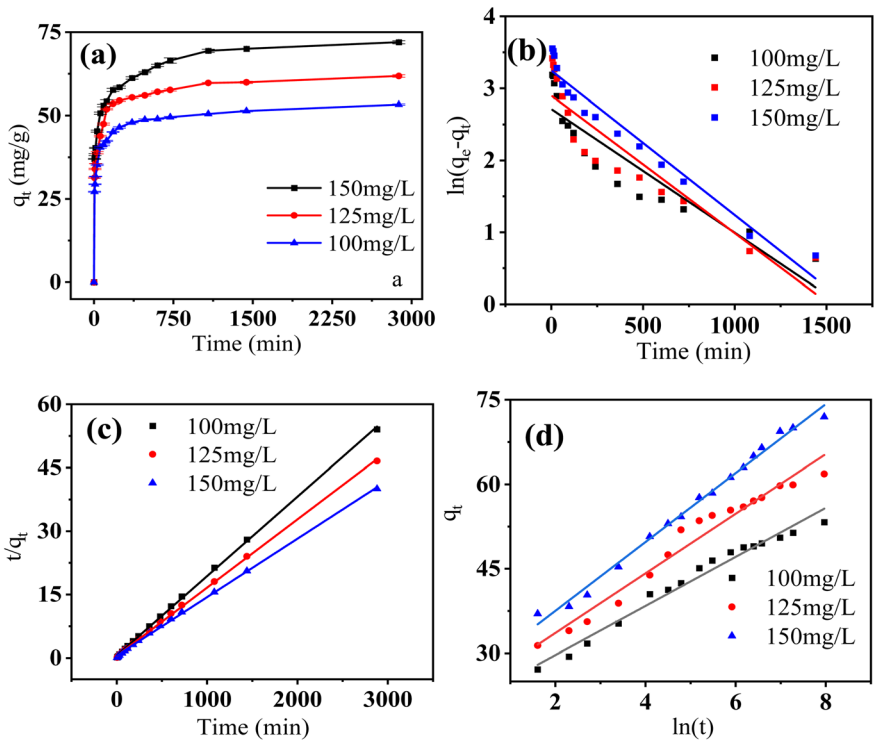

Fig. 7 Effect of contact time on Cr(VI) adsorption (a), linear fitting pseudofirst order kinetics (b), pseudosecond order kinetics (c) and Elovich model (d) (m = 0.02 g, pH = 4, T = 298 K).

Table 3 Kinetic parameters of Cr(VI) adsorption by FeS/CS@MIBWS

	Pseudo-first order			Pseudo-second order			Elovich		
C_0 mg L^{-1}	q_e	k_1	R^2	q_e	k_2	R^2	α	β	R^2
100	15.06	0.00172	0.825	53.16	0.000634	0.999	531.53	0.2293	0.9765
125	18.16	0.00191	0.835	61.84	0.000566	0.999	406.05	0.1887	0.9647
150	25.67	0.00127	0.948	72.20	0.000366	0.998	379.58	0.1634	0.9915

where c_e (mg L^{-1}) was the Cr(VI) concentration at equilibrium, q_m (mg g^{-1}) was the theoretical saturated Cr(VI) adsorption calculated from the Langmuir equation, b (L mg^{-1}) is the Langmuir constant, k_f and n are the Freundlich constant and exponent, respectively.

As shown in Fig. 8a, q_e was greater at higher temperatures than at lower temperatures for all the three reaction temperatures, indicating that higher temperatures resulted in improved Cr(VI) adsorption. Fig. 8b and c present the linearized fitting results from the two adopted models.

Table 4 shows that all the three correlation coefficients (R^2) of Langmuir model exceeded 0.99, whereas the highest correlation coefficient of Freundlich model was 0.939, suggesting Langmuir model was better to describe the Cr(VI) adsorption by FeS/CS@MIBWS, which is a monolayer adsorption process.

The influence of reaction temperature on Cr(VI) adsorption by FeS/CS@MIBWS and the feasibility of the process was studied using three thermodynamics including standard free energy change (ΔG^0), standard entropy change (ΔS^0), and standard enthalpy change (ΔH^0), which were obtained from eqn (6)–(8).[3]

$$\Delta G^0 = -RT\ln K_L \quad (6)$$

$$\Delta G^0 = \Delta H^0 - \Delta S^0 \quad (7)$$

$$\ln k = \frac{-\Delta G^0}{RT} = \frac{\Delta S^0}{R} - \frac{\Delta H^0}{RT} \quad (8)$$

Table 4 Isotherm parameters of Cr(VI) adsorption by FeS/CS@MIBWS at different temperatures

	Langmuir parameters			Freundlich parameters			Thermodynamic constants		
T (K)	q_m	b	R^2	k_f	n	R^2	ΔG^0	ΔH^0	ΔS^0
288	68.49	3.071	0.999	30.39	5.57	0.939	−1.40	39.41	0.14
298	78.74	1.806	0.999	36.11	5.44	0.853	−2.80		
308	92.68	1.251	0.998	43.36	5.22	0.707	−4.21		

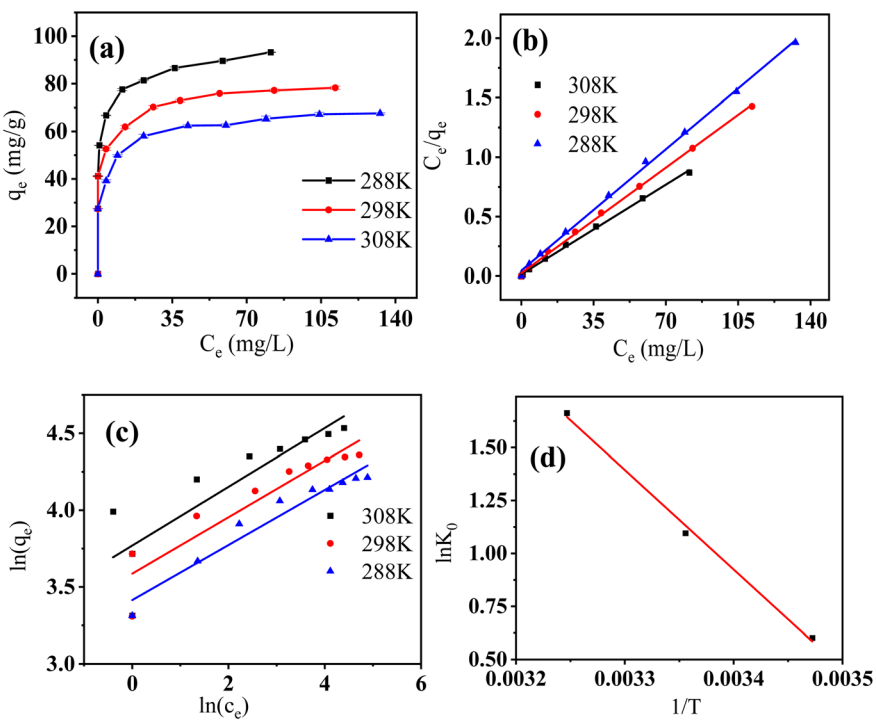

Fig. 8 The relationship between c_e and q_e under three reaction temperatures (a), linear fitting using Langmuir model (b), Freundlich model (c), and the relationship between $1/T$ and $\ln K_0$ for Cr(VI) adsorption by FeS/CS@MIBWS (d) (reaction time = 24 h, pH = 4).

Table 5 Comparison of monolayer Cr(VI) adsorption capacities of FeS/CS@MIBWS

Adsorbents	Moments (emu g^{-1})	Q_m (mg g^{-1})	Conditions (K & pH)	Ref.
Chitosan/polymethylmethacrylate	—	67.06	298 & 3	27
Magnetic zeolite/chitosan composites	18.67	28.47	303 & 3	46
Ethylamine modified chitosan carbonized rice husk composite beads	—	52.7	298 & 2	47
FCN-500	54.3	52.63	308 & 3	48
Magnetic activated carbon for	11.07	45.3	318 & 2	49
Magnetic zeolite/chitosan composite	16.83	21.25	288 & —	50
		23.76	303 & —	
		24.61	318 & —	
Ethylenediamine-modified cross-linked magnetic chitosan resin	—	51.81	293 & —	51
		48.78	303 & —	
		45.87	313 & —	
MnO_2/CS nanocomposite	—	61.56	298 & 2	52
FeS/CS@MIBWS	7.22	68.49	288 & 4	Current study
		78.74	298 & 4	
		92.68	308 & 4	

where K_L was a constant from Langmuir isotherm (L mol^{-1}); ΔS^0 and ΔH^0 were calculated from the relationship of ln K_L and $1/T$ shown in Fig. 8d, R is the ideal gas constant (8.314 J (mol^{-1} K^{-1})), T was the adsorption temperature (K). As shown in Table 4, ΔG^0 values for all the three reactions were negative and declined with the increasing temperatures, indicating the spontaneous nature of the adsorption process. The endothermic nature of the adsorption process was proved by the positive values of ΔH^0 and ΔS^0.

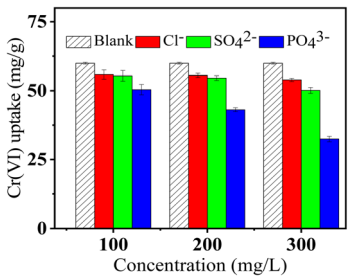

Fig. 9 The effect of coexisting ions on adsorption of Cr(VI) by FeS/CS@MIBWS (T = 298 K, pH = 4, C_0 = 50 mg L^{-1}).

Table 5 gives Cr(VI) adsorption capacities calculated from the Langmuir model for the modified chitosan adsorbents used in the existing documents and this study. The composite used in this study exhibited the fourth largest Cr(VI) uptake among the 9 composite, suggesting the adsorbent was an excellent material for Cr(VI) removal from water.

3.6 Effect of co-existing anions

The effect of common anions in water including Cl^-, SO_4^{2-} and PO_4^{3-} on Cr(VI) adsorption by FeS/CS@MIBWS was studied. As shown in Fig. 9, all the three anions impaired Cr(VI) uptake in the sequence of Cl^- < SO_4^{2-} < PO_4^{3-} with their increasing concentration, which was consistent with our prior findings and other recent research.[53] Due to the superimposition effect, the coexistence of the three anions resulted in lower Cr(VI) absorption than the solo effect of each anion.

3.7 Regeneration and reusability

Acetic acid and hydrochloric acid were used for FeS/CS@MIBWS regeneration (Fig. 10a). In comparison to 1 M $C_2(H_2O)_2$, all the three concentrations of HCl exhibited greater

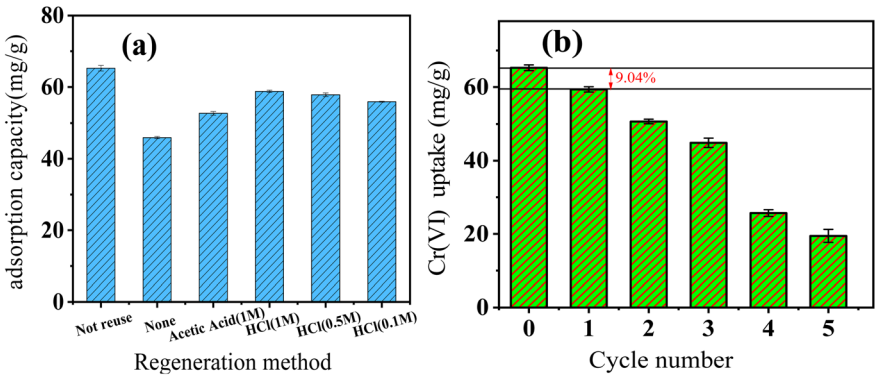

Fig. 10 Determination of regeneration reagent (a) and Cr(VI) uptake variation with reuse cycles (b).

regeneration effect, with 1 M HCl being the best for FeS/CS@MIBWS regeneration. As a results, 1 M HCl was used for FeS/CS@MIBWS regeneration.

As shown in Fig. 10b, there was 9.04% drop in Cr(VI) uptake after the first regeneration, and Cr(VI) uptake decreased by 70.2% after regeneration for 5 times, indicating the FeS/CS@MIBWS can be reused for times.

3.8 Mechanism exploration

As shown in Fig. 11, the bands at around 3369.0 cm^{-1}, 2924.0 cm^{-1}, 1712.5 cm^{-1}, 1648.8 cm^{-1},1376.0 cm^{-1} for FeS/CS@MIBWS belonged to NH_2 stretching,[54] symmetric CH vibration,[55] C=O stretching, symmetrical C=O stretching,[56] C–H bending,[57] respectively. The above-mentioned bands shifted to 3389.2 cm^{-1}, 2925.2 cm^{-1}, 1716.2 cm^{-1}, 1649.9 $cm^{-1}$and 1377.6 cm^{-1}, respectively, indicating their involvement into Cr(VI) elimination. The bands at 1031.7 cm^{-1}, 612.3 cm^{-1} and 477.3 cm^{-1} belonged to the primary amine C–N in chitosan,[58] α-Fe_2O_3 (ref. 59) and Fe–O asymmetric stretching,[60] respectively.

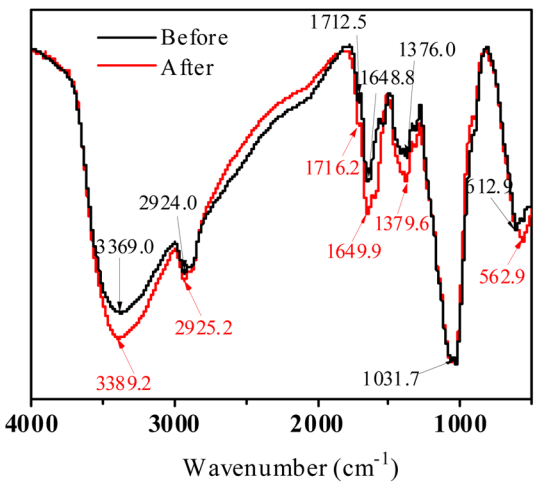

Fig. 11 FTIR spectra of FeS/CS@MIBWS before and after Cr(VI) adsorption.

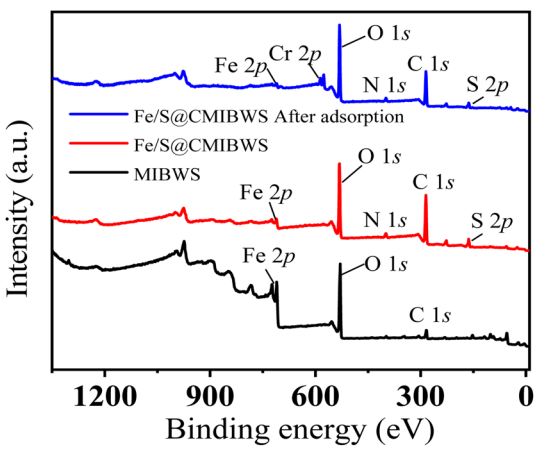

Fig. 12 The full XPS spectra of MIBWS, FeS/CS@MIBWS before and after Cr(VI) adsorption.

As shown in Fig. 12, the energy bands of Fe 2p, N 1s and S 2p appeared at the wide-scan spectrum of FeS/CS@MIBWS, indicating the chitosan and FeS were successfully loaded. The energy band of Cr 2p emerged after Cr(VI) adsorption, demonstrating the Cr(VI) was adsorbed on the surface of FeS/CS@MIBWS.

As shown in Fig. 13a, C 1s XPS spectrum of FeS/CS@MIBWS before Cr(VI) adsorption contained three functional groups with peaks at 283.7, 285.08 and 286.38 eV, corresponding to C=C, C–N and C–O, respectively.[61] Despite the fact that the bands of the three peaks did not altered after Cr(VI) adsorption, the peak area of C–N declined from 40.89% to 31.28%, and the peak area of C=C rose from 31.25% to 40.00% (Fig. 13b), respectively, indicating the participation of the carbon functional group into the Cr(VI) adsorption.

Fig. 13c shows that N 1s spectra contained three peaks at 398.1, 399.4 and 400.8 eV, respectively, which were attributed to –NH, $–NH_2$ and C–N, respectively,[62] indicating the presence of chitosan. After Cr(VI) adsorption, the peak area of –NH decreased from 63.48% to 26.16%, while the peak area of $–NH_2$ rose from 3.46% to 45.82%, respectively (Fig. 13d), indicating the nitrogen-containing functional group were protonated and participated in the Cr(VI) adsorption, which can be described by eqn (9)–(11).[63]

$$–NH + H^+ \rightarrow –NH_2 \quad (9)$$

$$–NH_2 + H^+ \rightarrow –NH_3^+ \quad (10)$$

$$–NH_3^+ + HCrO_4^- \rightarrow NH_3^+\cdots HCrO_4^- \quad (11)$$

S $2p_{1/2}$ and S $2p_{3/2}$ had peaks at approximately 166.8 eV and 162.5 eV, respectively (Fig. 13e). The binding energy of S $2p_{1/2}$ consisted two peaks at 162.3 eV and 163.3 eV, corresponding to FeS,[64] whereas, the binding energy of S $2p_{3/2}$ of SO_3^{2-} was found at 166.5 eV and 167.6 eV.[65] After Cr(VI) adsorption, the peak area of FeS fell from 80.98% to 72.96%, whereas the peak area of SO_3^{2-} increased from 19.20% to 27.04% (Fig. 13f), indicating the FeS formed during the participated into the Cr(VI) removal as electron donor, and the reaction can be expressed by equation.[66]

Fig. 13g shows the Fe 2p high resolution XPS spectra of FeS/CS@MIBWS before Cr(VI) adsorption. After Cr(VI) adsorption, the peaks attributed to both Fe^{3+} and Fe^{2+} shifted, and a new satellite peak emerged. Meanwhile, peak regions for Fe^{3+} increase from 30.37 to 43.13%, whereas, peak areas of Fe^{2+} declined from 69.63 to 56.87% (Fig. 13h). As a result, in conjunction with the study of Cr(VI) conversion, it is possible to assume that the Fe^{2+} in Fe_3O_4 in FeS/CS@MIBWS acted as reductant to reduce Cr(VI) into Cr(III), as stated by the following eqn (12)–(16).[45]

$$FeS + H^+ \rightarrow Fe^{2+} + HS^- \quad (12)$$

$$HS^- \rightarrow S^{2-} + H^+ \quad (13)$$

$$3Fe^{2+} + HCrO_4^- + 7H^+ \rightarrow 3Fe^{3+} + 2Cr^{3+} + 4H_2O \quad (14)$$

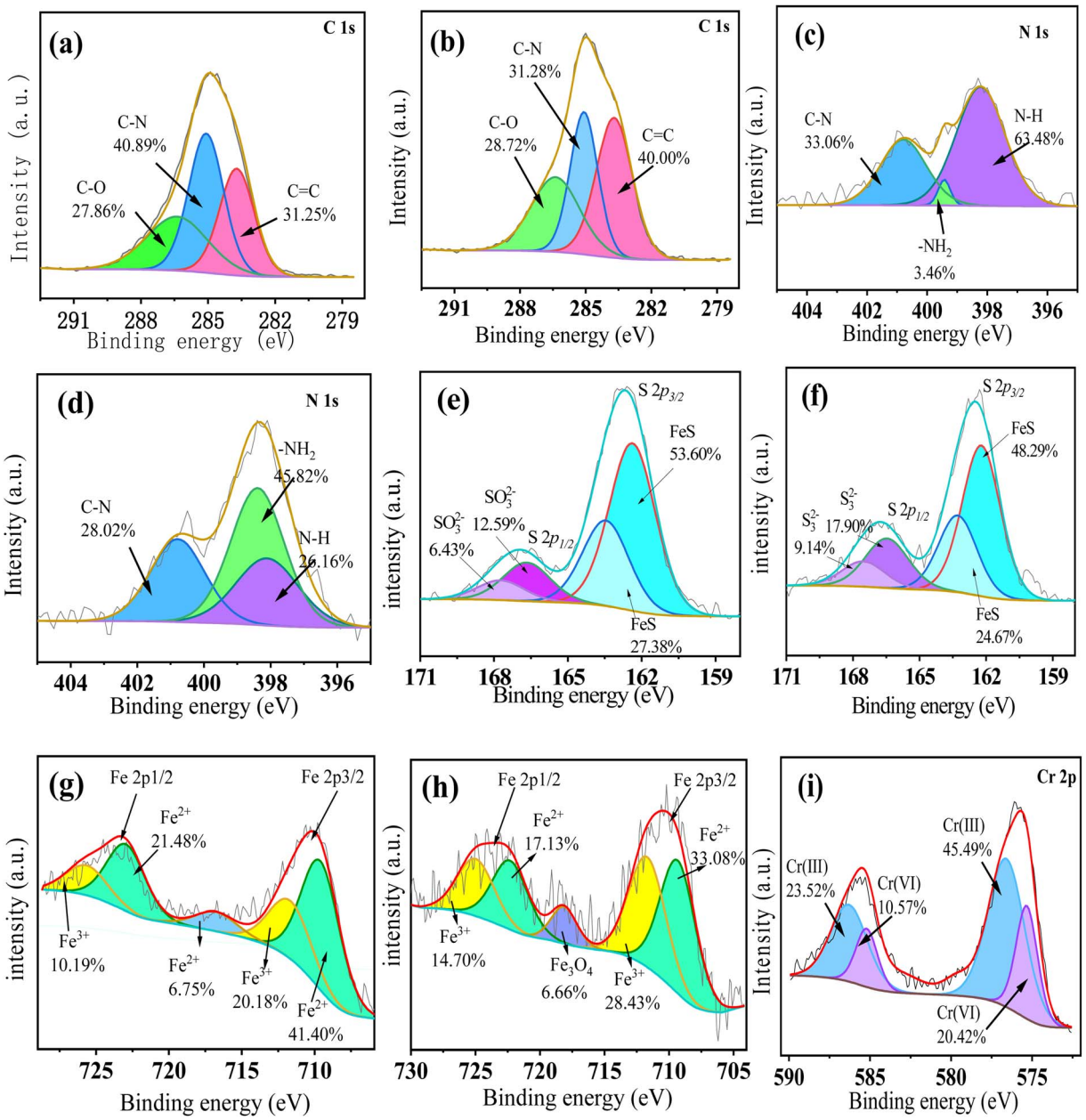

Fig. 13 The detail survey of C before (a) and after (b) Cr(VI) adsorption, N before (c) and after (d) Cr(VI) adsorption, S before (e) and after (f) Cr(VI) adsorption, Fe before (g) and after (h) Cr(VI) adsorption, Cr 2p after Cr(VI) adsorption (i).

$$3HS^- + 8HCrO_4^- + 29H^+ \rightarrow 3SO_4^{2-} + 8Cr^{3+} + 20H_2O \quad (15)$$

$$3S^{2-} + 2HCrO_4^- + 14H^+ \rightarrow 3S + 2Cr^{3+} + 8H_2O \quad (16)$$

As shown in Fig. 13i respectively, suggesting that Cr was adsorbed on the surface of FeS/CS@MIBWS.[67] The peaks at 575.3 eV and 585.3 eV corresponded to Cr $2p_{3/2}$ and Cr $2p_{1/2}$ of Cr(VI), and accounted for only 30.99% of the total peak area of Cr(VI). Peaks of 576.6 eV and 585.5 eV corresponded to Cr $2p_{3/2}$ and Cr $2p_{1/2}$ of Cr(III),[68] and its peak areas increased from 0 to 69.01% after Cr(VI) adsorption.

It can be concluded from the above analysis, physical and chemical adsorption, chelation and reduction of Cr(VI) into Cr(III) was participated the reaction.

4 Conclusion

In this study, MIBWS-based composite, namely FeS/CS@MIBWS was prepared by magnetized iron-based waterworks sludge, chitosan and FeS. The composite was adopted for a series of static Cr(VI) removal studies to investigate its Cr(VI) adsorption ability. Cr(VI) adsorption by the composite rose as the pH rose from 2 to 10. The pseudo-second order equation was more suitable for the description of Cr(VI) adsorption, and the Langmuir model fitted the experimental data better than the Freundlich model, the maximum uptake of aqueous Cr(VI) was 92.68 mg g^{-1} in 308 K. The main mechanism include physical and chemical adsorption, mainly the chelation and

reduction of Cr(VI) into Cr(III). The composite could be used to purify Cr(VI)-containing effluent.

Data availability

The data supporting this article have been included as part of the ESI.†

Author contributions

Jingxi Tie: conceptualization, methodology, writing – original draft, writing – review & editing; Weipeng Li: data curation, validation, writing – original draft; Xiaohan Duan: validation, visualization, writing – original draft; HuawenWang: investigation, validation; Shuli Liu: investigation, writing – original draft; Weigao Zhao: project administration, supervision, writing – review & editing. The manuscript was written through contributions of all authors. All authors have given approval to the final version of the manuscript.

Conflicts of interest

The authors declare no competing interests.

Acknowledgements

The authors gracefully thank for the final support by Henan Province Science and Technology Research and Development project (242102231015), Key Promotion Project of Henan Province (No. 232102321060) and Key R&D projects of Gansu Province in 2024 (24YFFK001).

References

1 A. Behera, S. P. Sahu, S. Kumar-Singh, B. Mahapatra and R. K. Patel, Polypyrrole modified zirconium (IV) phosphate nanocomposite: An effective adsorbent for Cr (VI) removal by adsorption-reduction mechanism, *Mater. Chem. Phys.*, 2022, **290**, 126540.

2 S. Y. Miao, J. R. Guo, Z. M. Deng, J. X. Yu and Y. R. Dai, Adsorption and reduction of Cr (VI) in water by iron-based metal-organic frameworks (Fe-MOFs) composite electrospun nanofibrous membranes, *J. Cleaner Prod.*, 2022, **370**, 133566.

3 J. X. Tie, W. P. Li, H. Y. Liu, K. Huang, X. Mi, M. H. Wei and L. J. Hou, Efficient adsorption and reduction of Cr(VI) by a novel polyaniline modified magnetic iron-based waterworks sludge from aqueous solution, *Chem. Eng. J.*, 2023, **451**(3), 137673.

4 J. J. Chang, J. Zhang, H. Wang, Y. F. Bai, Y. Liu, Y. Z. Bi, H. Z. Zhang, H. H. Chen, S. Barnie and H. J. Xie, Cr (VI) adsorption and reduction by magnetite-humic acid adsorption complexes under mildly acidic conditions: Synergistic/antagonistic mechanism and multi-step reaction model, *Chem. Eng. J.*, 2023, **451**, 138648.

5 J. C. Han, G. J. Chen, L. P. Qin and Y. Mu, Metal respiratory pathway-independent Cr isotope fractionation during Cr (VI) reduction by shewanella oneidensis MR-1, *Environ. Sci. Technol. Lett.*, 2017, **4**(11), 500–504.

6 R. S. Cutting, V. S. Coker, N. D. Telling, R. L. Kimber, C. I. Pearce, B. L. Ellis, R. S. Lawson, G. Van der Laan, R. A. D. Pattrick and D. J. Vaughan, Optimizing Cr (VI) and Tc (VII) remediation through nanoscale biomineral engineering, *Environ. Sci. Technol.*, 2010, **44**(7), 2577–2584.

7 S. P. Xia, Z. L. Song, P. Jeyakumar, S. M. Shaheen, J. Rinklebe, Y. S. Ok, N. Bolan and H. L. Wang, A critical review on bioremediation technologies for Cr (VI)-contaminated soils and wastewater, *Crit. Rev. Environ. Sci. Technol.*, 2019, **49**(12), 1027–1078.

8 K. Mukherjee, R. Saha, A. Ghosh and B. Saha, Chromium removal technologies, *Res. Chem. Intermed.*, 2013, **39**(6), 2267–2286.

9 A. S. Yusuff, M. A. Lala, K. A. Thompson-Yusuff and E. O. Babatunde, $ZnCl_2$-modified eucalyptus bark biochar as adsorbent: preparation, characterization and its application in adsorption of Cr (VI) from aqueous solutions, *S. Afr. J. Chem. Eng.*, 2022, **42**, 138–145.

10 N. Abdullah, N. Yusof, W. J. Lau, J. Jaafar and A. F. Ismail, Recent trends of heavy metal removal from water/wastewater by membrane technologies, *J. Ind. Eng. Chem.*, 2019, **76**, 17–38.

11 C. Pan, L. D. Troyer, P. Liao, J. G. Catalano, W. L. Li and D. E. Giammar, Effect of humic acid on the removal of chromium (VI) and the production of solids in iron electrocoagulation, *Environ. Sci. Technol.*, 2017, **51**(11), 6308–6318.

12 P. Sharma, J. Prakash, T. Palai and R. Kaushal, Surface functionalization of bamboo leave mediated synthesized SiO2 nanoparticles: Study of adsorption mechanism, isotherms and enhanced adsorption capacity for removal of Cr (VI) from aqueous solution, *Environ. Res.*, 2022, **214**, 113761.

13 Y. Zhao, W. K. Chang, Z. D. Huang, X. G. Feng, L. Ma, X. X. Qi and Z. H. Li, Enhanced removal of toxic Cr (VI) in tannery wastewater by photoelectrocatalysis with synthetic TiO2 hollow spheres, *Appl. Surf. Sci.*, 2017, **405**, 102–110.

14 C. B. Godiya, Y. H. Xiao and X. L. Lu, Amine functionalized sodium alginate hydrogel for efficient and rapid removal of methyl blue in water, *Int. J. Biol. Macromol.*, 2020, **144**, 671–681.

15 S. Yildiz and S. Sevinç, Heavy metal adsorption by dewatered iron-containing waste sludge, *Ecol. Chem. Eng. S*, 2018, **25**(3), 431–456.

16 J. J. Lian, F. J. Zhou, B. Bo Chen, M. Yang, S. S. Wang, Z. L. Liu and S. P. Niu, Enhanced adsorption of molybdenum(VI) onto drinking water treatment residues modified by thermal treatment and acid activation, *J. Cleaner Prod.*, 2020, **244**, 118719.

17 J. H. Wang, X. J. Han, Y. F. Ji and H. R. Ma, Adsorption of Cr(VI) from aqueous solution onto short-chain polyaniline/palygorskite composites, *Desalin. Water Treat.*, 2015, **56**(2), 356–365.

18 S. H. Shrestha, J. Kulandaivelu, K. Sharma, G. M. Jiang and Z. G. Yuan, Effects of dosing iron- and alum-containing

waterworks sludge on sulfide and phosphate removal in a pilot sewer, *J. Cleaner Prod.*, 2020, **387**, 118719.
19 A. Khan, Y. Huo, Z. Qu, Y. W. Liu, Z. H. Wang, Y. Chen and M. X. Huo, A facile calcination conversion of groundwater treatment sludge (GTS) as magnetic adsorbent for oxytetracycline adsorption, *Sci. Rep.*, 2021, **11**(1), 5276.
20 S. Y. Zhu, G. Dong, Y. Yu, J. K. Yang, W. Yang, W. Fan, D. D. Zhou, J. C. Liu, L. L. Zhang, M. X. Huo and Y. Wang, Hydrothermal synthesis of a magnetic adsorbent from wasted iron mud for effective removal of heavy metals from smelting wastewater, *Environ. Sci. Pollut. Res.*, 2018, **25**, 22710–22724.
21 E. Cheraghipour and M. Pakshir, Environmentally friendly magnetic chitosan nano-biocomposite for Cu(II) ions adsorption and magnetic nano-fluid hyperthermia: CCD-RSM design, *J. Environ. Chem. Eng.*, 2021, **9**(2), 104883.
22 A. H. Almarri, Chitosan composites for thionine dye adsorption, *Int. J. Environ. Anal. Chem.*, 2021, **1–12**, 1904915.
23 C. D. S. Cardoso and L. Vitali, Chitosan versus chitosan-vanillin modified: An evaluation of the competitive adsorption of five emerging contaminants, *Water, Air, Soil Pollut.*, 2021, **232**(5), 1–13.
24 X. L. Yu, J. Zhang and Y. Zheng, Perchlorate adsorption onto epichlorohydrin crosslinked chitosan hydrogel beads, *Sci. Total Environ.*, 2021, **761**, 143236.
25 S. L. Fan, Z. Q. Huang, Y. J. Zhang, H. Y. Hu, X. Q. Liang, S. X. Gong, J. Zhou and R. Tu, Magnetic chitosan-hydroxyapatite composite microspheres: Preparation, characterization, and application for the adsorption of phenolic substances, *Bioresour. Technol.*, 2019, **274**, 48–55.
26 V. N. Le, T. N. Tu and J. Kim, Facile synthesis of Cu-based metal-organic framework/chitosan composite granules for toluene adsorption, *Sep. Purif. Technol.*, 2023, **306**, 122718.
27 Z. Y. Li, T. T. Li, L. B. An, P. F. Fu, C. J. Gao and Z. M. Zhang, Highly efficient chromium(VI) adsorption with nanofibrous filter paper prepared through electrospinning chitosan/polymethylmethacrylate composite, *Carbohydr. Polym.*, 2016, **137**, 119–126.
28 Y. Yang, Y. H. Zhang, G. Y. Wang, Z. B. Yang, J. R. Xian, Y. X. Yang, T. Li, Y. L. Pu, Y. X. Jia, Y. Li, Z. Cheng, S. R. Zhang and X. X. Xu, Adsorption and reduction of Cr(VI) by a novel nanoscale FeS/chitosan/biochar composite from aqueous solution, *J. Environ. Chem. Eng.*, 2021, **9**(4), 105407.
29 H. P. Yang, M. Hong and S. Y. Chen, Removal of Cr(VI) with Nano-FeS and CMC-FeS and transport properties in porous media, *Environ. Technol.*, 2020, **41**(22), 2935–2945.
30 J. L. Liu, B. Q. Zhou, H. Zhang, J. Ma and W. B. Zhang, A novel biochar modified by chitosan-Fe/S for tetracycline adsorption and studies on site energy distribution, *Bioresour. Technol.*, 2019, **294**, 122152.
31 D. D. Shao, X. X. Wang, J. X. Li, Y. S. Huang, X. M. Ren, G. S. Hou and X. K. Wang, Reductive immobilization of uranium by PAAM-FeS/Fe3O4 magnetic composites, *Environ. Sci.: Water Res. Technol.*, 2015, **8**, 3155.
32 G. R. Liu, C. F. Song, Z. L. Huang, X. Jin, K. H. Cao, F. Y. Chen, B. H. Jin, R. Li and Q. Huang, Ultrasound enhanced destruction of tetracycline hydrochloride with peroxydisulfate oxidation over FeS/NBC catalyst: Governing factors, strengthening mechanism and degradation pathway, *Chemosphere*, 2023, **338**, 139418.
33 H. Y. Chen, P. F. Lv, Q. M. Liu, P. F. Tian, S. Y. Cao and S. J. Yuan, Bonding iron chalcogenides in a hierarchical structure for high-stability sodium storage, *J. Colloid Interface Sci.*, 2023, **637**, 251–261.
34 D. M. Feng, X. Zhang, Y. Sun and T. Y. Ma, Surface-defective FeS_2 for electrochemical NH_3 production under ambient conditions, *Nano Mater. Sci.*, 2020, **2**(2), 132–139.
35 C. T. Wei, M. X. Shen, K. L. Ai and L. H. Lu, Transformation from FeS/Fe_3C nanoparticles encased S, N dual doped carbon nanotubes to nanosheets for enhanced oxygen reduction performance, *Carbon*, 2017, **123**, 135–144.
36 S. C. Ma, Q. Cai, K. Lu, F. Liao and M. W. Shao, Bi-functional Au/FeS (Au/Co_3O_4) composite for in situ SERS monitoring and degradation of organic pollutants, *J. Nanopart. Res.*, 2016, **18**, 1–13.
37 S. T. Danalıoğlu, Ş. S. Bayazit, Ö. Kerkez-Kuyumcu and M. A. Salam, Efficient removal of antibiotics by a novel magnetic adsorbent: Magnetic activated carbon/chitosan (MACC) nanocomposite, *J. Mol. Liq.*, 2017, **240**, 589–596.
38 R. Varma and S. Vasudevan, Extraction, characterization, and antimicrobial activity of chitosan from horse mussel modiolus modiolus, *ACS Omega*, 2020, **5**(32), 20224–20230.
39 X. Zhong, Z. P. Lu, W. Liang and B. W. Hu, The magnetic covalent organic framework as a platform for high-performance extraction of Cr(VI) and bisphenol A from aqueous solution, *J. Hazard. Mater.*, 2020, **393**, 122353.
40 Z. M. Liu, G. Chen, L. C. Xu, F. P. Hu and X. Y. Duan, Removal of Cr(VI) from wastewater by a Novel adsorbent of magnetic goethite: Adsorption performance and adsorbent characterisation, *ChemistrySelect*, 2019, **4**, 13817–13827.
41 R. Borah, S. Banerjee and A. Kumar, Surface functionalization effects on structural, conformational, and optical properties of polyaniline nanofibers, *Synth. Met.*, 2014, **197**, 225–232.
42 Z. Lu, H. Zhang, A. Shahab, K. Zhang and H. Ullah, Comparative study on characterization and adsorption properties of phosphoric acid activated bio char and nitrogen-containing modified biochar employing Eucalyptus as a precursor, *J. Cleaner Prod.*, 2021, **12**, 127046.
43 C. B. Godiya, S. M. Sayed, Y. H. Xiao and X. L. Lu, Highly porous egg white/polyethyleneimine hydrogel for rapid removal ofheavy metal ions and catalysis in wastewater, *React. Funct. Polym.*, 2020, **149**, 104509.
44 J. Manuel, J. Salguero and R. P. Ramasamy, Synthesis and characterization of polyaniline nanofibers as cathode active material for sodium-ion battery, *J. Appl. Electrochem.*, 2019, **49**, 529–537.
45 C. B. Godiya, S. Kumarb and Y. H. Xiao, Amine functionalized egg albumin hydrogel with enhanced adsorption potential for diclofenac sodium in water, *J. Hazard. Mater.*, 2020, **393**, 122417.
46 X. Q. Liu, Y. Y. Zhang, Y. Liu and T. A. Zhang, Green method to synthesize magnetic zeolite/chitosan composites and

adsorption of hexavalent chromium from aqueous solutions, *Int. J. Biol. Macromol.*, 2022, **194**, 746–754.

47 S. Sugashini and K. M. M. S. Begum, Column adsorption studies for the removal of Cr(VI) ions by ethylamine modified chitosan carbonized rice husk composite beads with modelling and optimization, *J. Chem.*, 2012, **11**, 460971.

48 X. Liu, H. L. Liu, K. P. Cui, Z. L. Dai, B. Wang and R. Weerasooriya, Adsorption-Reduction of Cr(VI) with Magnetic Fe-C-N Composites, *Water*, 2023, **15**(12), 2290.

49 Z. Y. Wu, H. Zhang, E. Ali, A. Shahab, H. Y. Huang, H. Ullah and H. H. Zeng, Synthesis of novel magnetic activated carbon for effective Cr(VI) removal via synergistic adsorption and chemical reduction, *Environ. Technol. Innovat.*, 2023, **30**, 103092.

50 X. Q. Liu, Y. Liu and T. A. Zhang, Preparation of magnetic zeolite/chitosan composite using silane as modifier for adsorption of Cr(VI) from aqueous solutions, *J. Vinyl Addit. Technol.*, 2021, **27**, 640–654.

51 X. J. Hu, J. S. Wang, Y. G. Liu, X. Li, G. M. Zeng, Z. L. Bao, X. X. Zeng, A. W. Chen and F. Long, Adsorption of chromium (VI) by ethylenediamine-modified cross-linked magnetic chitosan resin: Isotherms, kinetics and thermodynamics, *J. Hazard. Mater.*, 2010, **185**(1), 306–314.

52 V. P. Dinh, M. D. Nguyen, Q. H. Nguyen, T. T. T. Do and L. V. Tan, Chitosan-MnO_2 nanocomposite for effective removal of Cr (VI) from aqueous solution, *Chemosphere*, 2020, **257**, 127147.

53 B. Mahanty and S. Mondal, Synthesis of Magnetic Biochar Using Agricultural Waste for the Separation of Cr(VI) From Aqueous Solution, *Arab. J. Sci. Eng.*, 2021, **46**, 10803–10818.

54 J. Monjane, D. Chemane, A. Zimba, P. Dimande and A. Uamusse, Production of chitosan from crab shells using an aqueous extract of wood ash for the deacetylation of chitin: An innovative, eco-friendly, and low-cost method, *Am. J. Polym. Sci. Techol.*, 2021, **7**(2), 29–37.

55 N. Ismillayli, S. Hadi, N. K. T. Dharmayani, R. K. Sanjaya and D. Hermanto, Characterization of alginate-chitosan membrane as potential edible film, *IOP Conf. Ser. Mater. Sci. Eng.*, 2020, **833**, 012073.

56 A. Raghatate, F. D. C. Vega, O. V. Meraz, K. Ahmadi, N. M. Chaudhari, D. S. A. Puthirath, N. Castaneda, P. M. Ajayan, J. M. H. Ramirez, V. Balan and F. C. R. Hernández, Sustainable biocomposites for structural applications with environmental affinity, *ACS Appl. Mater. Interfaces*, 2022, **14**(15), 17837–17848.

57 A. M. Bin, J. J. Lim, K. Shameli, N. A. Ibrahim and M. Y. Tay, Synthesis of silver nanoparticles in chitosan, gelatin and chitosan/gelatin bionanocomposites by a chemical reducing agent and their characterization, *Molecules*, 2011, **16**(9), 7237–7248.

58 D. W. Zhang, J. M. Wang, L. Ren, X. C. Meng, B. Y. Luan and Y. M. Zhang, A novel cationic-modified chitosan flocculant efficiently treats alkali-surfactant- polymer flooding-produced water, *Polym. Bull.*, 2023, **80**, 12865–12879.

59 O. A. Bulavchenko, A. A. Pochtar, E. Y. Gerasimov, A. V. Fedorov and V. V. Kaichev, Chemical and texture promoters in Cu-Fe-Al oxide nanocomposite catalysts for combustion of solid fuel gasification products, *Appl. Catal., A*, 2019, **590**, 117364.

60 A. Ramachandran, P. Anitha and S. Gnanavel, Structural and electronic impacts on corrosion inhibition activity of novel heterocyclic carboxamides derivatives on mild steel in 1 M HCl environment: Experimental and theoretical approaches, *J. Mol. Liq.*, 2022, **359**, 119218.

61 F. C. De-Godoi, E. Rodriguez-Castellon, E. Guibal and M. M. Beppu, An XPS study of chromate and vanadate sorption mechanism by chitosan membrane containing copper nanoparticles, *Chem. Eng. J.*, 2013, **234**, 423–429.

62 R. Bhatt, B. Sreedhar and P. Padmaja, Chitosan supramolecularly cross linked with trimesic acid-facile synthesis, characterization and evaluation of adsorption potential for chromium (VI), *Int. J. Biol. Macromol.*, 2017, **104**, 1254–1266.

63 L. L. Luo, S. Y. Cheng, L. H. Yue, Z. M. You and J. J. Cai, N-doped biochar from chitosan gel-like solution: Effect of hydrothermal temperature and superior aqueous Cr (VI) removal performance, *Colloids Surf., A*, 2022, **641**, 128426.

64 W. Q. Wu, Y. B. Li, J. Y. Jin, H. M. Wu, S. F. Wang and Q. H. Xia, A novel nonenzymatic electrochemical sensor based on 3D flower-like Ni7S6 for hydrogen peroxide and glucose, *Sens. Actuators, B*, 2016, **232**, 633–641.

65 V. A. Chanturiya, I. Z. Bunin and M. V. Ryazantseva, The main features of the natural sulphides surface modification under the impact of high-power electromagnetic pulses, *Inz. Miner.*, 2019, **21**(1/2), 123–127.

66 L. Kang, H. P. Yang, J. M. Wu and X. N. Liu, Facile integration of FeS and titanate nanotubes for efficient removal of total Cr from aqueous solution: Synergy in simultaneous reduction of Cr(VI) and adsorption of Cr(III), *J. Hazard. Mater.*, 2020, **398**, 122834.

67 X. Y. Lin, X. He, L. Lei, Y. F. Zhao, L. Z. Cui and G. Y. Wu, Development of ionic liquid filled chitosan capsules to remove Cr (VI) from acidic solution: adsorption properties and mechanism, *J. Environ. Chem. Eng.*, 2022, **10**(4), 108081.

68 C. S. Shen, H. Chen, S. S. Wu, Y. Z. Wen, L. N. Li, Z. J. Jiang, M. C. Li and W. P. Liu, Highly efficient detoxification of Cr (VI) by chitosan-Fe (III) complex: Process and mechanism studies, *J. Hazard. Mater.*, 2013, **244**, 689–697.